MedChemComm

Accepted Manuscript

ROYAL SOCIETY OF CHEMISTRY

www.rsc.org/medchemcomm

MedChemComm

RSCPublishing

ARTICLE

Structure-based approaches towards identification of fragments for the low-druggability ATAD2 bromodomain

Cite this: DOI: 10.1039/x0xx00000x

Received ooth January 2012,
Accepted ooth January 2012

DOI: 10.1039/x0xx00000x

www.rsc.org/

Apirat Chaikuad[a], Andrew M. Petros[c], Oleg Fedorov[b], Jing Xu[c], Stefan Knapp[a,b]

ABSTRACT: The transcriptional co-regulator ATAD2 is a prognostic marker for patient survival in many cancers. ATAD2 harbours a bromodomain which may offer an opportunity for pharmacological intervention, but its shallow, polar binding surface makes the development of inhibitors challenging. Here we optimized crystal transfer/soaking conditions enabling crystallographic fragment screening. We describe nine crystal structures of fragments including thymidine, a novel acetyl-lysine mimetic ligand and the evaluation of the binding properties of the identified fragments using NMR chemical shift perturbation experiments. The presented binding modes offer chemical starting points for the development of more potent ATAD2 inhibitors.

Introduction

ATAD2 (ATPases Associated with diverse cellular Activities), also called ANCCA (AAA+ nuclear co-regulator cancer associated) is a transcriptional regulator that harbours an AAA type ATPase domain and an acetyl-lysine protein interaction module of the bromodomain family. ATAD2 is highly expressed in testis[1] as well as in many diverse cancer types where its high expression levels have been strongly correlated with short patient survival and disease progression[1-4]. ATAD2 acts as a co-activator of several transcription factors that are key drivers of tumorigenesis including E2F family members[5], oestrogen receptors[6], the androgen-receptor[7] as well as MYC[8]. The association with MYC is particularly noteworthy as ATAD2 has been closely associated with expression of genes known to be transcriptionally up-regulated by MYC[9] leading to enhanced cell proliferation and resistance to apoptosis in an ATAD2-dependent manner. Taken together, the strong linkage of ATAD2 with cancer progression, its function as a co-regulator of key oncogenic drivers and the remarkable association of ATAD2 over-expression with patient survival makes a compelling case targeting this transcriptional co-activator for the treatment of cancer[10].

ATAD2 contains a single bromodomain, a protein interaction module that selectively recognizes acetyl-lysine containing sequence motifs. The human genome encodes 61 diverse bromodomains that are mainly present in chromatin associated proteins[11]. Interestingly, bromodomains have recently emerged as druggable protein interaction modules[12] and the strong association of some bromodomain containing proteins with disease development spawned a large number of drug discovery projects[13-15]. However, currently inhibitor development efforts have mainly focused on the BET family of bromodomain containing proteins for which a number of highly potent and selective inhibitors have been developed[16-21]. Despite the key role in tumorigenesis and disease progression, no inhibitors have been developed for the bromodomain of ATAD2. The polar and shallow binding pocket of the ATAD2 bromodomain suggests poor druggability of this acetyl-lysine interaction module[12]. Indeed, screening of ATAD2 against an acetyl-lysine mimetic library of potential bromodomain inhibitors developed in our laboratory yielded no potent inhibitor hits. We therefore used a fragment-based approach for the identification of chemical starting points that can be used for the development of more potent inhibitors. Here we present acetyl-lysine mimetic fragments and their high resolution crystal structures in complexes with ATAD2 as well as the evaluation of the binding properties of the most interesting fragments using NMR chemical shift perturbation experiments.

Results and discussion

Using the apo-structure of ATAD2[11], we solved the structure of an acetyl-lysine (Kac)/ATAD2 bromodomain complex to understand the structural requirements of ATAD2 acetyl-lysine

recognition. An initial co-crystal structure showed only weak density for the Kac ligand, possibly due to the high salt concentration required for ATAD2 crystallization that weakened interaction with this ligand. However, we were unable to identify alternative crystallization conditions which prompted us to consider crystal transfers to low-salt stabilizing solutions containing either PEG 3350 (polyethylene glycol of average molecular weight 3350) or 2-methyl-2,4-pentanediol (MPD) for soaking experiments[22]. Both polyoles yielded conditions in which the transferred ATAD2 crystals remained stabled. Combining the crystal transfer with Kac soaking yielded the acetyl-lysine complex structure, in which the ligand was well defined by electron density (**Figure 1a**). The acetyl-lysine binding mode was similar to the one observed in other bromodomain peptide or Kac complexes[11,23,24] and revealed the canonical hydrogen bond of the acetyl-lysine carbonyl with

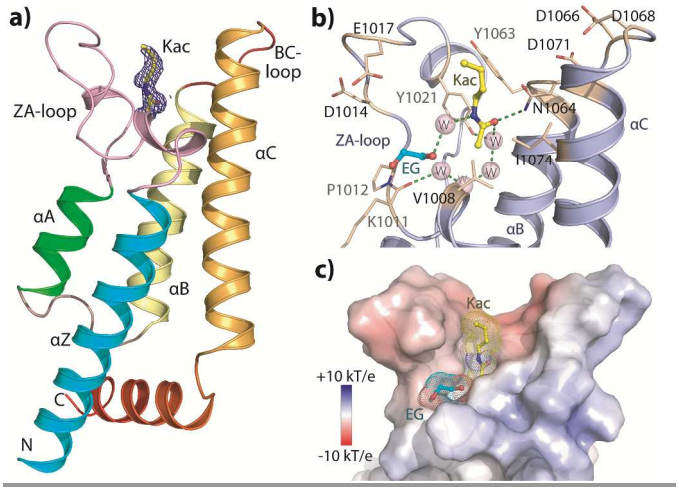

Figure 1: Overview of ATAD2 bromodomain in complex with acetyl-lysine. a) Ribbon representation of ATAD2 with the bound acetyl-lysine (Kac) shown in stick representation. The electron density shown around the ligand is $|2F_o|-|F_c|$ omitted map contoured at 1σ. **b)** Details of the interactions of ATAD2 with Kac. A bound ethylene glycol molecule (EG, highlighted in cyan) and water molecules (in pink spheres) are shown. **c)** Electrostatic surface representation of the acetyl-lysine binding pocket demonstrating its highly negatively-charged and shallow binding pocket properties.

a conserved asparagine (Asn1064) present in most bromodomains as well as a water-mediated hydrogen bond linking the Kac carbonyl with the ZA loop tyrosine (Tyr1021) and an intricate network of water molecules typically found at the bottom of the Kac binding pocket (**Figure 1b**). Interestingly, an ethylene glycol molecule that was present in the cryo-protectant bound adjacent the acetyl-lysine residue and interacted via a water-mediated hydrogen bond with the Kac amide suggesting that this moiety could guide growing the Kac fragment into more potent ligands (**Figure 1b**). As expected from the primary structure of ATAD2 the acetyl-lysine binding pocket and its flanking residues resulted in a highly polar binding site with largely negatively-charged ZA and BC loop regions (**Figure 1c**).

The charged binding pocket of ATAD2 posed a problem identifying ligands for this unusual bromodomain. We therefore initially used small polar solvent molecules that have been described acting as acetyl-lysine mimetic fragments for soaking experiments. The fragment library was dissolved in DMSO resulting in multiple co-crystal structures with this solvent. The sulfoxide oxygen acted in all cases as an acetyl-lysine mimetic ligand. Also MPD bound to ATAD2 assuming two closely related binding modes forming two hydrogen bonds with Asn1064 and a water-mediated hydrogen bond with Tyr1021 (**Figure 2a and 2b**). To avoid competition of the solvent with the binding of fragments we avoided therefore the use of MPD as a stabilizing agent during crystal transfer and used exclusively PEG-based stabilization solution. Other well-established acetyl-lysine mimetic fragments were successfully soaked into the ATAD2 binding pocket including the NMP ligand in an undiluted form (*N*-methyl-2-pyrrolidone) and 1-methylquinolin 2-one dissolved in 50:50 methanol:acetonitrile solvent (**Figure 2c and 2d**), which for the latter the DMSO-dissolved compound failed to co-crystallize most likely due to binding competition for the pocket of the solvent molecule.

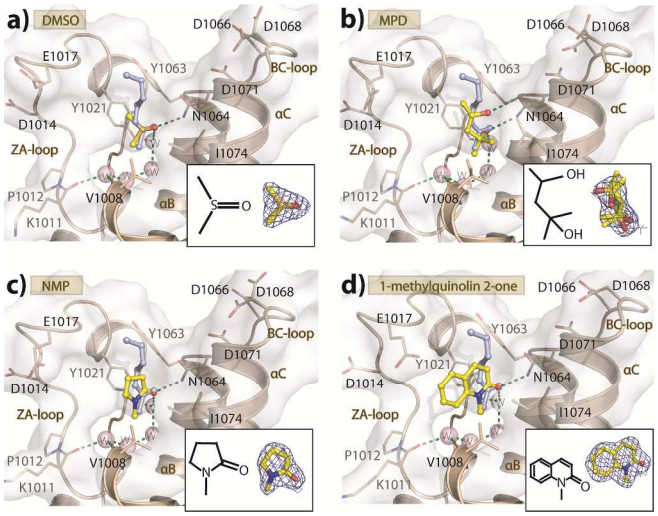

Figure 2 Structural details of the interaction of solvents and small fragments. Interaction with **a)** DMSO, **b)** 2-methyl-2,4-pentanediol (MPD, only main binding mode shown), **c)** *N*-methyl-2-pyrrolidone (NMP) and **d)** the small fragment 1-methylquinolin 2-one. All ligands are represented in yellow sticks with superimposed acetylated lysine highlighted by grey. Corresponding electron density maps ($|2F_o|-|F_c|$ contoured at 1σ) and the ligand structures are shown in the insets.

Ligand binding was associated with an ordering of some side chains increasing the level of enclosure of the binding site. Further screening of several addition acetyl-lysine mimetic ligands using compound concentrations in the range of 5-20 mM did not result in interpretable electron density maps (data

not shown). The results prompted us to hypothesize that the ATAD2 binding pocket, which is highly negatively-charged, might feasibly favour hydrophilic ligands.

Next, we further explored therefore a series of nucleosides and nucleobases in essence thymine, which contains a putative Kac mimetic moiety. This ligand is characterized by its excellent solubility in water allowing us to avoid the use of DMSO as solvent. Interestingly, thymine indeed bound to the ATAD2 acetyl-lysine binding pocket, forming the canonical Kac mimetic hydrogen bond with Asn1064 and the conserved water mediated hydrogen bond with Tyr1021 (**Figure 3a**). This prompted us to assess the binding of the nucleoside thymidine,

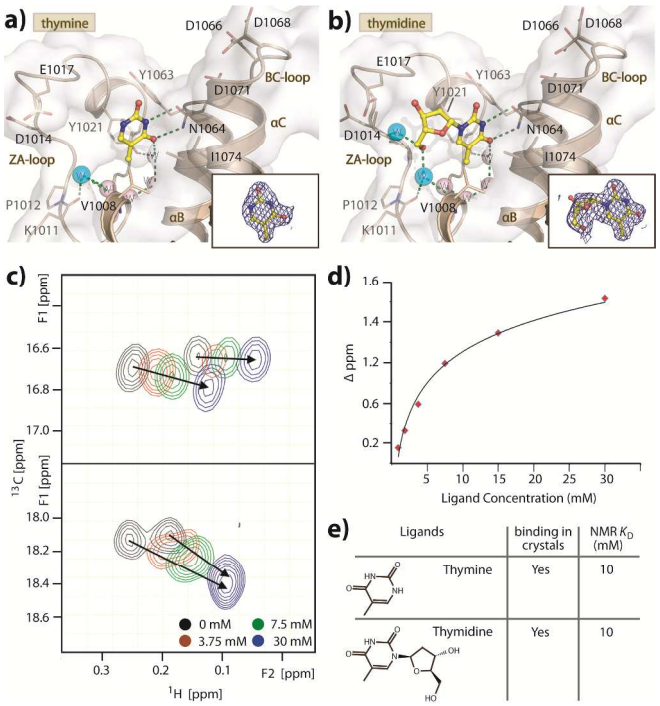

Figure 3: Binding of thymine and thymidine to the bromodomain of ATAD2. Structural details of the binding modes of thymine **(a)** and thymidine **(b)** represented as yellow stick models. The conserved network of water molecules are shown as pink sphere, while cyan spheres represent water molecules that are not part of the network and bridge interactions between the ligand and the protein ZA loop. The insets show electron density maps for the ligands ($|2Fo|-|Fc|$ contoured at 1σ). **c)** NMR titration of ATAD2 with thymidine. Two selected sections of the ^{13}C-HSQC spectra (500 MHz) in the presence of thymidine at different concentrations are shown. Arrows highlight chemical shift changes of cross-peaks as a result of ligand binding. **d)** Dose dependence of the chemical shift perturbations as a result of the binding of thymidine to ATAD2. **e)** Summary of the crystal transfer/soaking binding experiments and the estimated K_ds for thymine and thymidine based on NMR titration experiments.

which contains the deoxyribose decoration which, assuming that the thymine binding mode is conserved in the nucleoside complex, would protrude into pocket occupied by ethylene glycol in the Kac complex. The electron density map obtained from the ligand soaking experiment confirmed this hypothesis (**Figure 3b**). Interestingly, structural comparison with the Kac-ATAD2 complex showed that the oxygen atom of the thymidine sugar ring was accommodated in the position of the water molecule that bridged the interaction between the bound ethylene glycol and Kac while the 5'-hydroxyl group was oriented towards the solvent exposed pocket occupied by the ethylene glycol. Here, the 5'-hydroxyl group formed interactions to the ZA loop mediated by two water molecules leading to hydrogen bond networks between the ligand and the main chain atoms of Lys1011 and Val1008 as well as Asp1014. One of these bridging water molecules was also observed in the thymine complex but was not linked to the ligand due to the lack of the sugar moiety (**Figure 3a and 3b**). The 3'-hydroxyl group was located adjacent to an acidic patch of the ZA loop (Asp1014, Asp1016 and Glu1017), however no contact between this moiety and the protein was observed with its high crystallographic B-values suggesting also its flexibility. With the success in obtaining the complex structures, we sought to determine the affinities of these two compounds using NMR chemical shift perturbation experiments monitoring the chemical shifts of ^{13}C-methyl labeled ATAD2 (**Figure 3c**). Non-linear least squares fits of the dose dependency of the chemical shifts resulted in the K_d values of approximately 10 mM for both thymine and thymidine ligands (**Figure 3d and 3e**).

Next we expanded the ligand series by examining the binding of other related, commercially available thymidine nucleoside analogues with diverse modifications at the sugar group. Of the seven compounds tested (**Figure 4a**), the crystal transfer/soaking approach identified the interactions of two further nucleosides: the 5-methyl uridine and 3'-deoxythymidine, which exhibited full occupancy in the complex structures (**Figure 4b and 4c**). Interestingly, NMR titration experiments suggested the dissociation constants (K_d) of 21 and 18 mM for the 5-methyl uridine and 3'-deoxythymidine nucleosides, respectively, which were slightly weaker than the interactions of thymine or thymidine to ATAD2. Analyses of the structures revealed that the contacts between these two nucleosides with the protein were remarkably similar to that of thymidine, albeit with the differences noted for the water-mediated interactions between the 5'-hydroxyl group and the ZA loop (**Figure 4b and 4c**). Unlike two bound water molecules observed for the thymidine complex, the 5-methyl uridine- and 3'-deoxythymidine-ATAD2 complexes contained only one bound water molecule, and they were also positioned differently in these two structures. It is likely that the loss of water mediated interactions in the 5-methyl uridine and 3'-deoxythymidine complexes resulted in slightly weaker interactions of these ligands. In addition, similar to the thymidine complex the 2'- and 3'-hydroxyl groups of 5-methyl uridine were oriented towards the ZA loop polar surface patches but did not form any specific interactions with any ATAD2 residues.

It is to note also that among the thymidine nucleoside analogues tested in the soaking experiments zudovidine was another compound that showed binding in the crystals, but the weak electron density map did not allow a confident, accurate placement of this ligand, thus without a final model. To verify

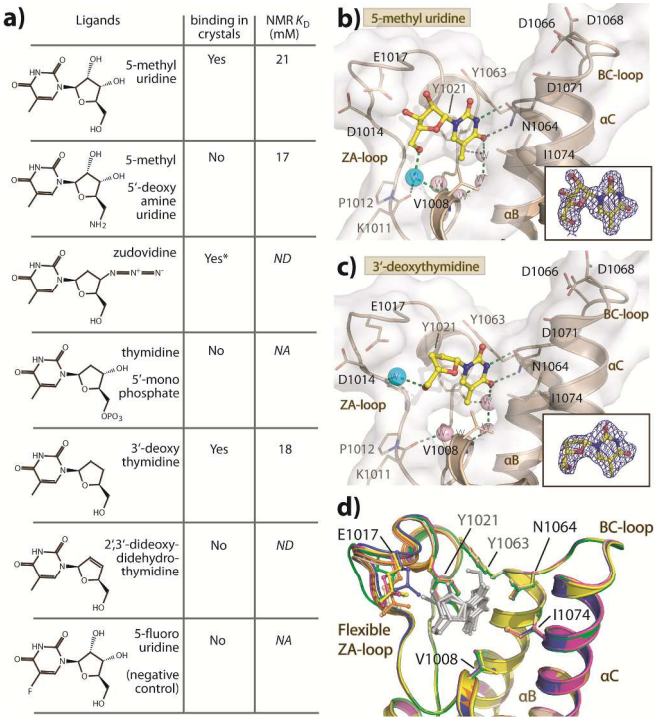

Figure 4 Binding of thymidine nucleoside analogues to ATAD2. a) Summary of thymidine nucleoside analogues tested for binding to ATAD2 using fragment screening and quantitative NMR chemical shift perturbations. * denotes weak electron density map for the sugar ring for zudovidine and therefore no final structural model obtained; *ND*, not determined; *NA,* not applicable however binding detected but likely with the K_d values much larger than the highest tested concentration of 30 mM. Structural details of interactions between **b)** 5-methyl uridine and **c)** 3'-deoxythymidine (both depicted as yellow sticks) and the ATAD2 bromodomain. The conserved water network is displayed as pink spheres, while the water molecules that mediate the interactions between the bound ligand and the ZA loop are shown as cyan spheres. The insets show $|2F_o|-|F_c|$ electron density maps contoured at 1σ for the bound nucleosides. **d)** Superimposition of the nucleobase-, nucleoside- and Kac-ATAD2 complexes revealed flexibility of the ZA loop upon binding to diverse ligands.

if the crystal transfer and soaking experiment was to some extent reliable, 5-fluoro uridine, which was not expected to bind to the bromodomain due to the lack of an acetyl-lysine mimetic methyl group, was used as a negative control and indeed did not interact in the ATAD2 crystals. Furthermore, a nucleotide did also not bind to the ATAD2 bromodomain. This can be explained by the non-compatible charge and potentially the larger size of the phosphate extension that is feasibly repelled by acidic residues located in the ATAD2 bromodomain Kac binding site, essentially at the pockets around the ZA loop. In general, the NMR titrations were in good agreement with the crystal transfer/soaking experiments. We were however unable to obtain the complex structure of the 5-methyl 5'-deoxyamine uridine which showed a K_d of 17 mM. The 5'-amine should fit well into the ATAD2 binding site and we can therefore not explain why the structure determination of this complex has been unsuccessful. Superimposition of all ATAD2 complexes presented in this study revealed a rather rigid bromodomain binding site. However, flexibility of the ZA loop and different conformations of the acidic side chains within this region (Asp1014, Asp1016 and Glu1017) were observed, suggesting some degree of domain plasticity induced by the studied ligands (**Figure 4d)**. Such structural feature may be taken into consideration upon further designs of more potent ATAD2 inhibitors. The nucleobase thymine represents an attractive acetyl-lysine mimetic moiety for ATAD2 whereas extension of this fragment by a sugar moiety does not increase affinity further. Indeed, the ribose rings in the nucleoside complexes make little direct contact with the ATAD2 bromodomain. The binding surface of the acetyl-lysine peptide binding site of ATAD2 is highly negatively charged and it is likely that addition of basic or polar extension groups to the thymine scaffold will potentially be more beneficial for increasing binding affinity than the tested sugar substitutions.

Conclusions

The developed and optimized crystal transfer/soaking approaches for crystallographic studies together with the NMR screening technology presented here offer a possible platform for structure-based design of more potent ATAD2 inhibitors. This is exemplified by the identification of the nucleobase thymine, a novel acetyl-lysine mimetic, including its several analogues as the possible ATAD2 ligands. In addition, the complex structures enable understanding of the negatively-charged, flexible nature of the ATAD2 pocket around the ZA loop, a region commonly targeted by bromodomain inhibitors. Although exhibiting only weak affinities, these fragments may offer starting points for synthetic efforts targeting this therapeutically-important bromodomain which is an ongoing activity in our laboratories.

Experimental

Protein purification and structure determination

The recombinant ATAD2 protein was expressed, purified and crystallized in its apo-form as previously described[11]. For transfer/soaking experiments, the crystals were transferred into the stabilizing/soaking solution, containing either i) 45-50% MPD, 0.1 M bis-tris pH 5.5 and 0.1 M ammonium phosphate or ii) 28-32% PEG 3350, 50 mM bis-tris pH 5.5, 50 mM ammonium phosphate and 20% ethylene glycol. Fragments were supplemented in the soaking solution at 20-50 mM concentration (10% for NMP). Soaking time was varied from 4-

9 hours. Diffraction data, collected in-house on Rigaku FR-E Superbright®, were processed and scaled with MOSFLM[25] and Scala implemented in the CCP4 suite[26], respectively. The structure determination was achieved by molecular replacement using Phaser[27] and the ATAD2 apo coordinates as a search model[11]. All structures were subjected to manual model building in COOT[28] and refinement using Refmac[29] with optimized TLS groups defined by the TLSMD server[30]. The final models were verified for their geometric correctness with MOLPROBITY[31]. The data collection and refinement statistics are summarized in **Supplementary Table 1**.

NMR Titrations

The bromodomain from human ATAD2 (981-1108) was expressed in *E. coli* strain BL21 (DE3) using the pET28b vector. The recombinant protein which was ^{13}C-labeled at the methyl groups of leucine, valine, isoleucine (δ only), and methionine was used for all NMR titrations. This labelling pattern was achieved by growing cells on minimal media which had been supplemented with ^{13}C-labeled α-ketovalerate (100 mg/L), ^{13}C-labeled α-ketobutyrate (50 mg/L) and ^{13}C-methyl-labeled methionine (50 mg/L). Soluble protein was purified by Ni^{2+}-affinity chromatography. All NMR spectra were collected at 25 ºC on a Bruker DRX500 spectrometer with a cryoprobe, on protein samples dissolved in 50 mM Tris pH 8.5, 1 mM TCEP, 100% ^2H_2O. For each NMR titration the ligand was first added as a dry powder to a 100 uM protein solution to give a final ligand concentration of 30 mM. This initial sample was then diluted with the protein solution to yield samples which all had 100 uM protein and 15, 7.5, 3.75, 1.875 and 0.9375 mM ligand. ^{13}C-HSQC spectra were recorded on each of the protein/ligand solutions along with the apo protein as a reference. The chemical shift for a particular methyl cross-peak was then measured as a function of ligand concentration. Dissociation constants were calculated by fitting the change in chemical shift compared to the apo-protein versus added ligand to a simple two site (on/off) binding model.

Acknowledgements

SK and OF are grateful for financial support by the SGC, a registered charity (number 1097737) that receives funds from AbbVie, Bayer, Boehringer Ingelheim, the Canada Foundation for Innovation, the Canadian Institutes for Health Research, Genome Canada, GlaxoSmithKline, Janssen, Lilly Canada, the Novartis Research Foundation, the Ontario Ministry of Economic Development and Innovation, Pfizer, Takeda, and the Wellcome Trust [092809/Z/10/Z]. AC has been supported by the European Union FP7 Grant No. 278568 "PRIMES"

Notes and references

[a] Nuffield Department of Clinical Medicine, SGC, University of Oxford, Oxford OX3 7DQ.
[b] Nuffield Department of Clinical Medicine, Target Discovery Institute, University of Oxford, Oxford OX3 7FZ.
[c] Abvvie, 1 North Waukegan Road, North Chicago, IL, 60064-6100, USA

Electronic Supplementary Information (ESI) available**: Supplementary table 1**: Crystallographic data collection and refinement statistics. See DOI: 10.1039/b000000x/

The atomic coordinates and structure factors have been deposited in the Protein Data Bank under accession codes: 4QSP, 4QSQ, 4QSR, 4QSS, 4QST, 4QSU, 4QSV, 4QSW and 4QSX.

1. C. Caron, C. Lestrat, S. Marsal, E. Escoffier, S. Curtet, V. Virolle, P. Barbry, A. Debernardi, C. Brambilla, E. Brambilla, S. Rousseaux and S. Khochbin, Oncogene, 2010, 29, 5171-5181.
2. X. Chen, S. T. Cheung, S. So, S. T. Fan, C. Barry, J. Higgins, K. M. Lai, J. Ji, S. Dudoit, I. O. Ng, M. Van De Rijn, D. Botstein and P. O. Brown, Molecular biology of the cell, 2002, 13, 1929-1939.
3. L. J. van 't Veer, H. Dai, M. J. van de Vijver, Y. D. He, A. A. Hart, M. Mao, H. L. Peterse, K. van der Kooy, M. J. Marton, A. T. Witteveen, G. J. Schreiber, R. M. Kerkhoven, C. Roberts, P. S. Linsley, R. Bernards and S. H. Friend, Nature, 2002, 415, 530-536.
4. E. V. Kalashnikova, A. S. Revenko, A. T. Gemo, N. P. Andrews, C. G. Tepper, J. X. Zou, R. D. Cardiff, A. D. Borowsky and H. W. Chen, Cancer research, 2010, 70, 9402-9412.
5. A. S. Revenko, E. V. Kalashnikova, A. T. Gemo, J. X. Zou and H. W. Chen, Molecular and cellular biology, 2010, 30, 5260-5272.
6. J. X. Zou, A. S. Revenko, L. B. Li, A. T. Gemo and H. W. Chen, Proceedings of the National Academy of Sciences of the United States of America, 2007, 104, 18067-18072.
7. J. X. Zou, L. Guo, A. S. Revenko, C. G. Tepper, A. T. Gemo, H. J. Kung and H. W. Chen, Cancer research, 2009, 69, 3339-3346.
8. M. Ciro, E. Prosperini, M. Quarto, U. Grazini, J. Walfridsson, F. McBlane, P. Nucifero, G. Pacchiana, M. Capra, J. Christensen and K. Helin, Cancer research, 2009, 69, 8491-8498.
9. M. B. Raeder, E. Birkeland, J. Trovik, C. Krakstad, S. Shehata, S. Schumacher, T. I. Zack, A. Krohn, H. M. Werner, S. E. Moody, E. Wik, I. M. Stefansson, F. Holst, A. M. Oyan, P. Tamayo, J. P. Mesirov, K. H. Kalland, L. A. Akslen, R. Simon, R. Beroukhim and H. B. Salvesen, PloS one, 2013, 8, e54873.
10. F. Boussouar, M. Jamshidikia, Y. Morozumi, S. Rousseaux and S. Khochbin, Biochimica et biophysica acta, 2013, 1829, 1010-1014.
11. P. Filippakopoulos, S. Picaud, M. Mangos, T. Keates, J. P. Lambert, D. Barsyte-Lovejoy, I. Felletar, R. Volkmer, S. Muller, T. Pawson, A. C. Gingras, C. H. Arrowsmith and S. Knapp, Cell, 2012, 149, 214-231.
12. L. R. Vidler, N. Brown, S. Knapp and S. Hoelder, Journal of medicinal chemistry, 2012, 55, 7346-7359.
13. S. Muller, P. Filippakopoulos and S. Knapp, Expert reviews in molecular medicine, 2011, 13, e29.
14. P. Filippakopoulos and S. Knapp, Nature reviews. Drug discovery, 2014, 13, 337-356.
15. S. Knapp and H. Weinmann, ChemMedChem, 2013, 8, 1885-1891.
16. P. Filippakopoulos, J. Qi, S. Picaud, Y. Shen, W. B. Smith, O. Fedorov, E. M. Morse, T. Keates, T. T. Hickman, I. Felletar, M. Philpott, S. Munro, M. R. McKeown, Y. Wang, A. L. Christie, N. West, M. J. Cameron, B. Schwartz, T. D. Heightman, N. La Thangue, C. A. French, O. Wiest, A. L. Kung, S. Knapp and J. E. Bradner, Nature, 2010, 468, 1067-1073.

17. E. Nicodeme, K. L. Jeffrey, U. Schaefer, S. Beinke, S. Dewell, C. W. Chung, R. Chandwani, I. Marazzi, P. Wilson, H. Coste, J. White, J. Kirilovsky, C. M. Rice, J. M. Lora, R. K. Prinjha, K. Lee and A. Tarakhovsky, Nature, 2010, 468, 1119-1123.
18. M. A. Dawson, R. K. Prinjha, A. Dittmann, G. Giotopoulos, M. Bantscheff, W. I. Chan, S. C. Robson, C. W. Chung, C. Hopf, M. M. Savitski, C. Huthmacher, E. Gudgin, D. Lugo, S. Beinke, T. D. Chapman, E. J. Roberts, P. E. Soden, K. R. Auger, O. Mirguet, K. Doehner, R. Delwel, A. K. Burnett, P. Jeffrey, G. Drewes, K. Lee, B. J. Huntly and T. Kouzarides, Nature, 2011, 478, 529-533.
19. S. Picaud, D. Da Costa, A. Thanasopoulou, P. Filippakopoulos, P. V. Fish, M. Philpott, O. Fedorov, P. Brennan, M. E. Bunnage, D. R. Owen, J. E. Bradner, P. Taniere, B. O'Sullivan, S. Muller, J. Schwaller, T. Stankovic and S. Knapp, Cancer research, 2013, 73, 3336-3346.
20. S. Picaud, C. Wells, I. Felletar, D. Brotherton, S. Martin, P. Savitsky, B. Diez-Dacal, M. Philpott, C. Bountra, H. Lingard, O. Fedorov, S. Muller, P. E. Brennan, S. Knapp and P. Filippakopoulos, Proceedings of the National Academy of Sciences of the United States of America, 2013, 110, 19754-19759.
21. P. Ciceri, S. Muller, A. O'Mahony, O. Fedorov, P. Filippakopoulos, J. P. Hunt, E. A. Lasater, G. Pallares, S. Picaud, C. Wells, S. Martin, L. M. Wodicka, N. P. Shah, D. K. Treiber and S. Knapp, Nat Chem Biol, 2014, 10, 305-312.
22. R. K. Wierenga, J. P. Zeelen and M. E. M. Noble, J Cryst Growth, 1992, 122, 231-234.
23. D. J. Owen, P. Ornaghi, J. C. Yang, N. Lowe, P. R. Evans, P. Ballario, D. Neuhaus, P. Filetici and A. A. Travers, The EMBO journal, 2000, 19, 6141-6149.
24. F. M. Ferguson, O. Fedorov, A. Chaikuad, M. Philpott, J. R. Muniz, I. Felletar, F. von Delft, T. Heightman, S. Knapp, C. Abell and A. Ciulli, Journal of medicinal chemistry, 2013, 56, 10183-10187.
25. T. G. Battye, L. Kontogiannis, O. Johnson, H. R. Powell and A. G. Leslie, Acta crystallographica. Section D, Biological crystallography, 2011, 67, 271-281.
26. N. Collaborative Computational Project, Acta crystallographica. Section D, Biological crystallography, 1994, 50, 760-763.
27. A. J. McCoy, R. W. Grosse-Kunstleve, P. D. Adams, M. D. Winn, L. C. Storoni and R. J. Read, Journal of applied crystallography, 2007, 40, 658-674.
28. P. Emsley, B. Lohkamp, W. G. Scott and K. Cowtan, Acta crystallographica. Section D, Biological crystallography, 2010, 66, 486-501.
29. G. N. Murshudov, A. A. Vagin and E. J. Dodson, Acta crystallographica. Section D, Biological crystallography, 1997, 53, 240-255.
30. J. Painter and E. A. Merritt, Acta crystallographica. Section D, Biological crystallography, 2006, 62, 439-450.
31. I. W. Davis, A. Leaver-Fay, V. B. Chen, J. N. Block, G. J. Kapral, X. Wang, L. W. Murray, W. B. Arendall, 3rd, J. Snoeyink, J. S. Richardson and D. C. Richardson, Nucleic Acids Res, 2007, 35, W375-383.